Journal of Naval Architecture and Marine Engineering
June, 2024
http://dx.doi.org/10.3329/jname.v21i1.69871 *http://www.banglajol.info*

NUMERICAL INVESTIGATION OF 3-D WING MOVING OVER FREE SURFACE IN WATER OF FINITE DEPTH

S. Bal[1]
[1]Department of Naval Architecture, Istanbul Technical University, Ayazaga Campus, Maslak- Sariyer, Istanbul, Turkiye, Email: sbal@itu.edu.tr

Abstract:

Three-dimensional (3-D) wing moving steadily over free water surface with the effects of finite depth has been investigated numerically using an iterative boundary element method (IBEM), which was developed for cavitating 3-D hydrofoils advancing under a free surface. The IBEM has been modified and extended for this purpose. The water is incompressible, inviscid and the flow is irrotational. All variables and equations are made dimensionless. In this way the convergence of the numerical scheme is achieved very quickly and consistently. The IBEM is based on Green's theorem. The wing part of problem (including its wake), the free surface problem and the bottom surface problem are solved separately with the effects on each other. The 3-D wing surface, the bottom surface and free surface are modeled with constant strength source and doublet panels. The kinematic boundary condition is applied both on the wing surface and on the bottom surface. On the other hand, the linearized kinematic and dynamic combined condition is applied on the free water surface. The method is first applied to a rectangular wing with a high aspect ratio to compare the pressure distribution on mid-section strip with that of two-dimensional method. Later, the IBEM is applied to a tapered swept-back wing and the effects of finite depth on wing performance have been examined. It is noted that the reduced water depth causes an increase in Kelvin wedge angle, wave height and wave length compared to the infinite depth case. It is also found that a decrease in the depth of bottom surface causes an increase in the loading on the wing.

Keywords: Wing, free surface, finite depth, wave drag, lift.

NOMENCLATURE

AR	aspect ratio	NW	total number of panels on free surface
c_{tip}	chord length at tip	p	pressure
c_{root}	chord length at tip	p_0	reference pressure
C_D	drag coefficient	s	span
C_L	lift coefficient	S_B	bottom surface
C_p	pressure coefficient	S_{FS}	free surface
d	depth of finite bottom from free surface	S_W	wing surface
D	drag force	S_{WK}	wake surface
f_{max}	maximum camber	t_{max}	maximum thickness
Fr_c	chord-based Froude number (=U/(gc_{root})$^{0.5}$)	U	velocity of incoming flow
Fr_h	clearance-based Froude number (=U/(gh)$^{0.5}$)	***Greek symbols***	
g	gravitational acceleration	α	angle of attack
h	clearance between wing and calm free surface	Φ	total potential
$IBEM$	iterative boundary element method	ϕ	perturbation potential
L	lift force	ρ	density of water
NBS	number of panels on bottom surface	ζ	wave elevation
NFS	number of panels on free surface		

1813-8535 (Print), 2070-8998 (Online) Received on: Nov., 2023

1. Introduction

Marine crafts utilizing the wing-in-ground (WIG) effect, along with certain very high-speed marine vehicles, can exploit air wings to either partially or completely lift the weight of the vehicle. The aerodynamic performance of these wings holds significant practical importance for high-speed air-assisted boats, whether navigating in deep water or in water of finite depth. The vertical clearance between the wing and free surface, as well as the depth of finite bottom from free water surface, can significantly impact the performance (lift and drag forces) of these supporting wings. This study aims to numerically investigate the performance of three-dimensional (3-D) wings moving at a constant speed above free surface in water of finite depth using an iterative boundary element method (IBEM) developed previously for cavitating hydrofoils operating under a free surface. This problem was not previously addressed to the author's knowledge.

Previous studies have extensively examined two-dimensional (2-D) and 3-D hydrofoils operating either under or piercing the free surface, with or without cavitation (Carabineanu, 2014; Chen, 2012; Sun and Wu, 2022; Bal 2007a, Bal 2007b). However, the research on 2-D or 3-D WIGs travelling over a free water surface is limited compared to the studies on hydrofoils operating beneath the free surface. A recent study successfully tackled the flow problem around a 2-D WIG moving closely to a free water surface (Zong et al., 2012). It emphasized the significance emergence of the WIG effect when the clearance between free surface and WIG craft is small enough. Additionally, a lifting surface theory for 3-D WIG crafts with free surface effects under subsonic flow conditions was previously developed (Liang and Zong, 2011), demonstrating the significant occurrence of the WIG effect when the clearance is sufficiently small, giving the findings in the 2-D case. Further investigations into WIG problems in both 2-D and 3-D cases were conducted in (Barber, 2007), revealing varying behaviors of the free surface deformation based on Froude numbers. Notably, a small change in the shape of free surface deformation was observed for higher Froude numbers. For very high Froude numbers, (say Froude number, 14), the free surface beneath the foil rises up. A similar conclusion was also made in (Grundy, 1986). The WIG craft moving steadily that is close to the free water surface, has been investigated numerically both in two-dimensional (2-D) and three-dimensional (3-D) cases in (Bal, 2016). The problem has been solved by an IBEM in deep water. The numerical results have been validated with experiments. Moreover, research explored the endplate effects on the performance of 3D wings operating above free surface in (Jung et al., 2012), highlighting a potential decrease in induced drag due to end plates. A combined aero-hydrodynamic flow simulation for a ram wing moving above free water surface steadily was described in (Matveev, 2013). The aerodynamic performance parameters of a ram wing and associated water surface deformations were presented. In another study, IBEM has been applied to different types of WIGs, such as inverted and tapered ones (Bal, 2018). The effects of dihedral and sweep angles on the performance of WIGs were discussed. For a comprehensive understanding of WIG crafts and the development of WIG technology, extensive resources and detailed information are presented in review surveys such as those by (Rozhdestvensky, 2010; Rozhdestvensky, 2006).

However, none of the aforementioned studies have incorporated the effects of finite bottom on the performance of WIGs into their calculations. In this paper, the numerical method (IBEM) previously developed for cavitating or non-cavitating hydrofoils working below a free surface has been adapted and expanded to accommodate 3-D WIGs moving over the free water surface. IBEM employs Green's theorem (Green's second identity) to construct an integral equation, which is then divided into three components: (i) the wing portion, including its wake, (ii) the free surface portion and (iii) the finite bottom portion. These three components are addressed individually, with their interdependencies considered iteratively. The three isolated problems make a connection each other by their potential values. Specifically, the potential induced by the wing on the free and the bottom surfaces, by free surface on wing and bottom surfaces, and by bottom surface on wing and free surfaces are all accounted for on the right-hand sides of their corresponding integral equation. The validity of results of present IBEM has been previously confirmed through experiments and comparison with those of other methods (Bal et al., 2001; Bal and Kinnas, 2002; Bal, 2016), obviating the need for repetition in this study. The method has recently been utilized to examine the impact of curved tips on the performance of cavitating hydrofoils (Bal, 2023), yielding very satisfactory results for practical applications. Here, initially a rectangular wing with aspect ratio (AR=10) was selected and the pressure distribution on the mid-section was compared with that of 2-D panel method - a comparison not previously conducted. Subsequently, the method was applied to a 3-D tapered swept back wing geometry with the angle of attack of five degrees. The effects of finite depth on lift coefficient, drag coefficient, pressure distribution and the free surface deformation were thoroughly investigated.

In the subsequent sections, the mathematical model of the problem is presented for comprehensive understanding. The numerical procedure and IBEM are then introduced in a brief form, along with a demonstration of the

algorithm (flow diagram) of the numerical method. Following this, numerical results for a validation test and for a tapered swept back wing are presented, accompanied by discussion on the effects of shallow water on the results. Finally, some remarks are made in Conclusion section.

2. Mathematical Model

Consider a wing positioned above free water surface with finite depth. A uniform inflow, U as depicted in Fig. 1, is passing this wing. Oxyz cartesian coordinate right-handed system is defined, where the x-axis is positive in the inflow direction and the z-axis is indicating upwards as positive (Fig. 1). The origin is situated at the intersection point of mid-span and mid-chord length in the y axis and x axis, respectively. The wing above undisturbed free surface is situated at z = h, where the vertical distance between the free surface and wing is h, and the vertical distance between the horizontal flat bottom surface and mean free surface is d. The water is incompressible, inviscid and the flow is both irrotational and steady. All variables and equations are dimensionless, made by using U and c_{root}, where c_{root} is described and illustrated in Fig. 1. The mathematical model was elaborated in detail in previous works (Bal et al., 2001; Bal, 2002), and is presented here in a brief form for the sake of completeness.

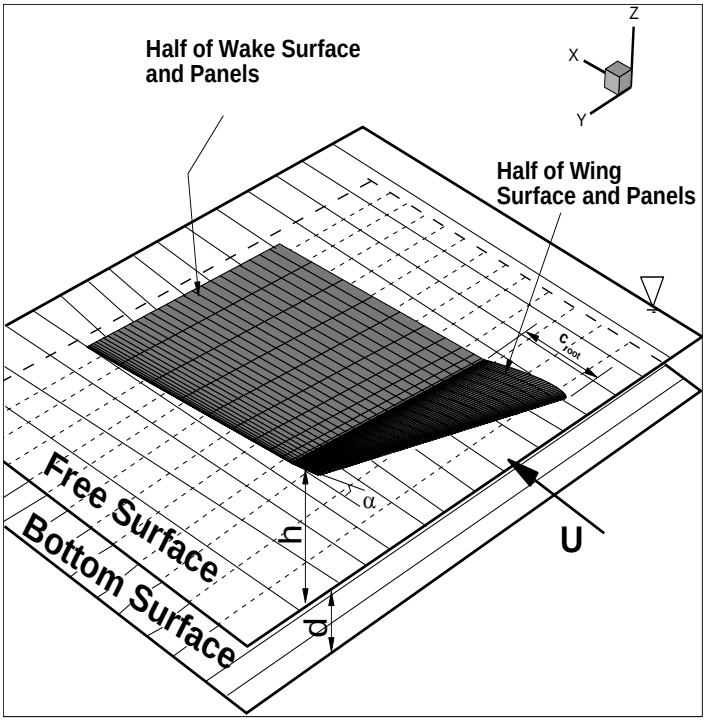

Fig. 1: Definition of coordinate system for 3-D wing problem. Half of wing is shown due to symmetry.

Both the total potential,Φ(x, z) and the perturbation potential, ϕ(x, z) must satisfy the Laplace's equation (mass conservation) in the fluid domain:

$$\nabla^2\Phi = 0 \text{ and } \nabla^2\phi = 0 \tag{1}$$

Here, in non-dimensional form $\Phi = \frac{x}{c_{root}} + \phi$.

The perturbation potential, ϕ must satisfy the following boundary conditions:

1-) Kinematic condition on wing surface: The flow velocity must be align with (parallel to) the surface of the wing, ensuring that the total velocity perpendicular to the wing surface is zero:

$$\frac{\partial\phi}{\partial n} = -\frac{|\overrightarrow{n_x}|}{c_{root}} \quad \text{on } S_W \tag{2}$$

Here, $\vec{n}$ represents the unit normal vector on the wing surface directed towards the air. S_W denotes the wing surface.

2-) Kutta and wake condition: Finite velocity values must be obtained at the trailing edge of the wing by enforcing the Kutta condition:

$$\nabla\phi = \text{finite}; \quad \text{at TE} \tag{3}$$

TE means trailing edge. This condition ensures that the flow quits the wing at its TE. The force must be zero on the wake surface and this condition must also be fulfilled. The strengths of doublet at the trailing edge are carried to the surface of wake to ensure zero pressure jump, leading to an iterative Morino's Kutta condition:

$$\phi^+ - \phi^- = \Delta\phi_w \tag{4}$$

where ϕ^+ and ϕ^- are the potential values at the up and down wake planes of the wing, respectively. Further details are presented in (Kinnas and Hsin, 1992).

3-) Linearized and combined free surface condition: Combining the kinematic and dynamic free surface conditions and neglecting higher-order terms yield the linearized free surface equation in non-dimensional form as follows:

$$\frac{\partial^2\phi}{\partial x^2} + Fr_c^{-2}\frac{\partial\phi}{\partial z} = 0 \quad \text{on} \quad z = 0 \tag{5}$$

Here, Fr_c represents the Froude number ($Fr_c = \frac{U}{\sqrt{gc_{root}}}$) and g is the acceleration of gravitation. Note that this condition does not account for wave breaking and wave spray if they occur. The corresponding linearized wave elevation is given by:

$$\zeta = -Fr_c^2\frac{\partial\phi}{\partial x} \tag{6}$$

Here, ζ denotes non-dimensional wave elevation.

4-) Radiation condition: Upstream waves must not occur on the free surface, implying that both the first and second-order derivatives of the perturbation potential value with respect to x-coordinate must be zero as demonstrated in (Bal et al., 2001):

$$\frac{\partial^2\phi}{\partial x^2} = \frac{\partial\phi}{\partial x} = 0 \quad \text{as} \quad x \to -\infty \tag{7}$$

5-) Finite-depth condition: The normal velocity on bottom surface must be zero. Since the incoming velocity does not contribute to the normal velocity on finite bottom surface, this equation can be expressed as:

$$\frac{\partial\phi}{\partial z} = 0 \quad \text{on } S_B \tag{8}$$

3. Numerical Solution by IBEM

The perturbation potential on the wing surface, free surface and bottom surface can be expressed as (Katz and Plotkin, 2001) using Green's third identity:

$$2\pi\phi = \int_{S_W+S_{FS}+S_B}\left(\phi\frac{\partial G}{\partial n} - \frac{\partial\phi}{\partial n}G\right)dS + \int_{S_{WK}}\Delta\phi_W\frac{\partial G}{\partial n^+}dS \tag{9}$$

where S_W, S_{WK}, S_{FS} and S_B are the boundaries of the wing surface, its wake surface, free surface and bottom surface, respectively. The Green function is G=1/r for the 3-D wing problem. The distance is r between the singularity (doublet or source) point and the field point. The potential jump is defined $\Delta\phi_W$, over the wake surface

as given in Equation (4), and the unit vector perpendicular to the surface of wake is n^+, pointing positive z direction. In the present study, the iterative method mainly presented primarily in (Bal, 2011) is modified and applied to solve the Equation (9). The problem here is separated to three isolated parts: (1) the wing part, including its wake, (2) the free surface part and (3) the bottom surface part. The potential value induced by the wing surface and its wake surface, ϕ_W, can be written as (Katz and Plotkin, 2001):

$$2\pi\phi_W = \int_{S_W}\left(\phi\frac{\partial G}{\partial n} - \frac{\partial \phi}{\partial n}G\right)dS + \int_{S_{WK}}\Delta\phi_W\frac{\partial G}{\partial n^+}dS \tag{10}$$

The potential values in the fluid domain induced by the free surface and the bottom surface, ϕ_{FS} and ϕ_{BS} can be written as:

$$2\pi\phi_{FS} = \int_{S_{FS}}\left(\phi\frac{\partial G}{\partial n} - \frac{\partial \phi}{\partial n}G\right)dS \tag{11}$$

$$2\pi\phi_B = \int_{S_B}\left(\phi\frac{\partial G}{\partial n} - \frac{\partial \phi}{\partial n}G\right)dS \tag{12}$$

By substituting the Equation (11) and Equation (12) into Equation (9), the integral equation for the wing surface, including its wake can be written as follows:

$$2\pi\phi_W = \int_{S_W}\left(\phi\frac{\partial G}{\partial n} - \frac{\partial \phi}{\partial n}G\right)dS + \int_{S_{WK}}\Delta\phi_W\frac{\partial G}{\partial n^+}dS + 4\pi(\phi_{FS} + \phi_B) \tag{13}$$

and by similarly substituting Equation (10) and Equation (12) into Equation (9), the integral equation for the free surface can be written as follows:

$$2\pi\phi_{FS} = \int_{S_{FS}}\left(\phi\frac{\partial G}{\partial n} - \frac{\partial \phi}{\partial n}G\right)dS + 4\pi(\phi_W + \phi_B) \tag{14}$$

Similarly, by substituting Equation (10) and Equation (11) into Equation (9), the integral equation for the bottom surface can also be written as follows:

$$2\pi\phi_B = \int_{B}\left(\phi\frac{\partial G}{\partial n} - \frac{\partial \phi}{\partial n}G\right)dS + 4\pi(\phi_W + \phi_{FS}) \tag{15}$$

When the kinematic condition on the wing surface and the bottom surface and the free surface condition have all been applied, the Equations (13), (14) and (15) can be rewritten as follows:

$$2\pi\phi_W = \int_{S_W}\left(\phi\frac{\partial G}{\partial n} + n_x G\right)dS + \int_{S_{WK}}\Delta\phi_W\frac{\partial G}{\partial n^+}dS + 4\pi(\phi_{FS} + \phi_B) \tag{16}$$

$$2\pi\phi_{FS} = \int_{S_{FS}}\left(\phi\frac{\partial G}{\partial n} + Fr_c^2\frac{\partial^2\phi}{\partial x^2}G\right)dS + 4\pi(\phi_W + \phi_B) \tag{17}$$

$$2\pi\phi_B = \int_{S_B}\left(\phi\frac{\partial G}{\partial n}\right)dS + 4\pi(\phi_W + \phi_{FS}) \tag{18}$$

where, the x-component of the unit normal vector on the wing surface is n_x. The integral Equations (15-17) can be solved in an iterative manner using a Dirichlet type panel method. The potentials $\boldsymbol{\phi}_W$, $\boldsymbol{\phi}_{FS}$ and $\boldsymbol{\phi}_B$ are modified during the iterative process. The iteration process ends up with when the difference between the potential values of two running iterations is less than a certain specified value. The wing surface, free surface and bottom surface are discretized into small rectangular elements (panels). Both the constant strength source and dipole singularities are distributed on the panels. The algorithm (flow diagram) of the numerical method is shown in Fig. 2. Two advantages of this method are as follows:

1-) Solutions to isolated problems are much simpler to manage and organize numerically compared to tackling the entire problem as a whole,

2-) Each isolated problem necessitates less computation time and less memory compared to solving the entire problem. Consequently, the total computation time for iterative process is significantly reduced to solving the full-problem.

Further details on the method are presented in (Bal et al., 2001, Bal 2011).

4. Numerical Results and Discussion

The existing IBEM has undergone through validation to predict flow characteristics around fully submerged non-cavitating and cavitating hydrofoils without free surface effects. This validation involved extensive convergence testing as well as the comparison to experimental data and other numerical methods (Bal and Kinnas, 2002). Thus, they are not repeated here. This study presents the results of a numerical IBEM applied to a rectangular wing with AR of 10 (AR=span/chord ratio), comparing them with those obtained using a 2-D numerical panel method (Bal, et al., 2001). The rectangular wing has NACA0012 sections along its span-wise direction, facilitating a direct comparison of the pressure distributions on the center section of wing with those of a 2-D NACA0012 section at an angle of attack of α=5º. This comparison was not previously conducted. The wing comprises a total of 4800 panels (80 panels along chord-wise direction and 60 along span-wise direction) as shown in Fig. 3, with symmetry applied to half of the wing with respect to the span.

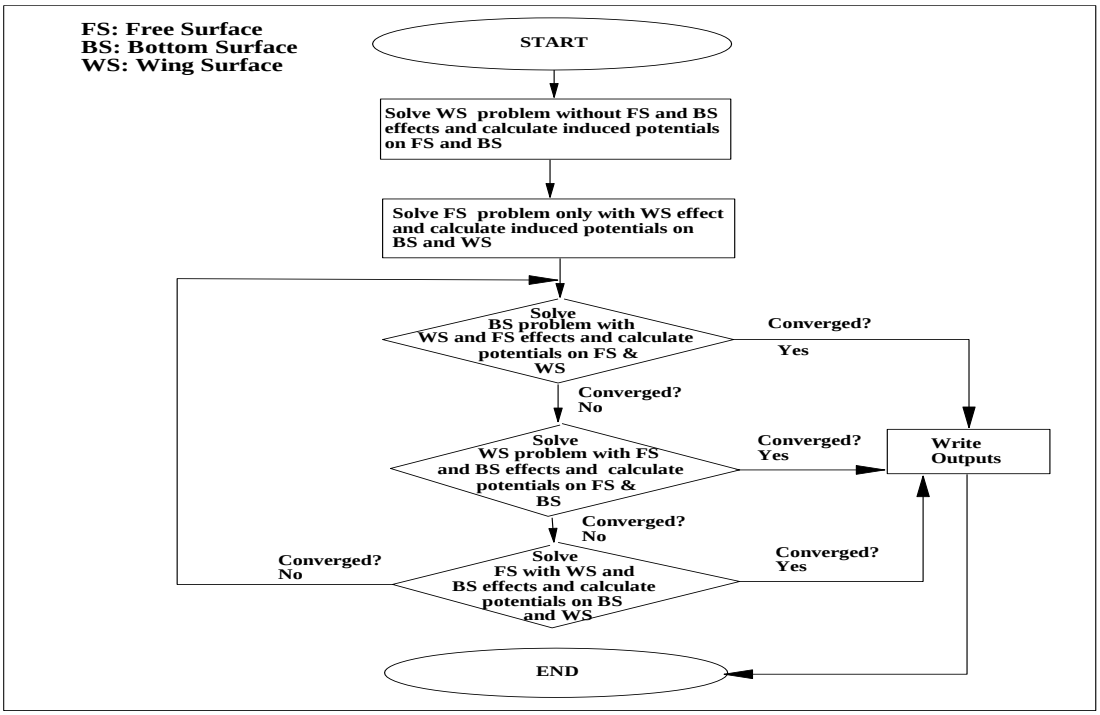

Fig. 2: Flow diagram of present IBEM.

In Fig. 4, the dimensionless pressure distribution $C_p=(p-p_0) / (0.5\rho U^2)$ for mid-section strip is demonstrated as compared with that of 2-D panel method in unbounded flow domain. A very good compromise has been found between two solutions except a very small region near leading edge. This is also somehow a validation of the method. Subsequently, another rectangular wing with aspect ratio of 5 is examined to illustrate the effects of finite-depth solely on mid-section pressure distribution. The wing features NACA0012 sections along its span-wise direction. The number of panels on the bottom surface is 2000, (100 panels in the x direction and 20 panels in the y direction). Free surface effects are not considered in this specific case. As shown in Fig. 5, the finite-depth results in an increase in loading (lift coefficient) on the wing, as expected. The lift coefficient and drag coefficient ($C_L = \frac{L}{\frac{1}{2}\rho AU^2}$, $C_D = \frac{D}{\frac{1}{2}\rho AU^2}$, L: lift force, D: drag force, A: planform wing area) in unbounded domain for this wing are calculated as C_L=0.2238 and C_D=0.0042, respectively. For the case where the depth-to-chord ratio (d/c) equals 0.25, the lift coefficient and drag coefficient for this wing are calculated as C_L=0.2888 and C_D=0.0022,

respectively. A shallower finite depth induces a higher lift coefficient while concurrently reducing the drag coefficient. This observation aligns with the pressure distributions shown in Fig. 5.

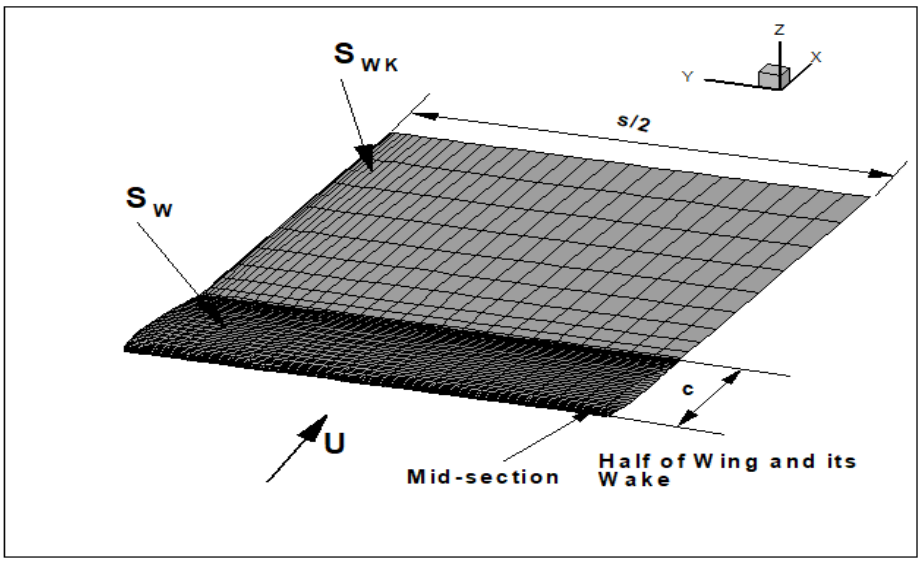

Fig. 3: Panels on rectangular wing and its wake, AR=10, α=5º (Half of wing is shown due to symmetry).

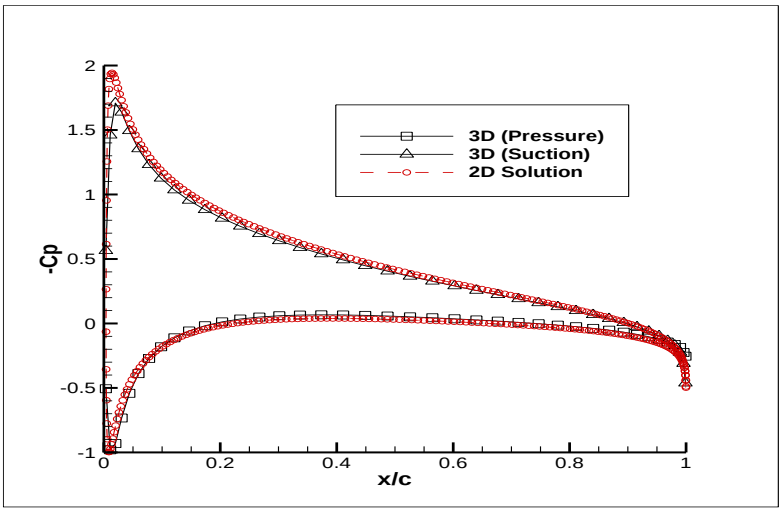

Fig. 4: Comparison of pressure distribution on the mid-section of 3-D wing and 2-D solution.

Subsequently, a tapered swept back wing with a taper ratio (c_{root}/c_{tip}=3) and sweep angle (λ=19.5º) is chosen, modeled with an aspect ratio (aspect ratio=s^2/A; where A is the planform area of the wing) of 3.75. The chord length at mid-section and at tip, as well as the span of the wing are denoted as c_{root}, c_{tip} and s, respectively, as illustrated in Fig. 6. Additional geometrical details of the wing are provided in Table 1. The wing features symmetrical (no camber) NACA four digit-sections with varying thickness distribution along the span-wise direction. The root section adheres to NACA0012 while the tip section is of zero thickness. The flow around the wing is initially simulated numerically for infinite depth case without considering free surface effects (e.g., in an unbounded flow domain). These analyses are conducted at the angle of attack, α=5°. The number of panels on the half wing surface is 2400, (80 panels along the chord-wise direction and 30 panels along half-span-wise direction) as shown for half of the wing due to symmetry with respect to span in Fig. 6. Full cosine spacing in the chord direction and half cosine spacing in the half-span direction are applied for the simulations. The number of panels on both the free surface and bottom surface is consistent, set at 2000, (100 panels in the x-direction and 20 in the y-direction). These types of panel distributions and the number of panels on the surfaces of each sub problem (wing surface, free surface, and bottom surface) remain consistent for all subsequent simulations.

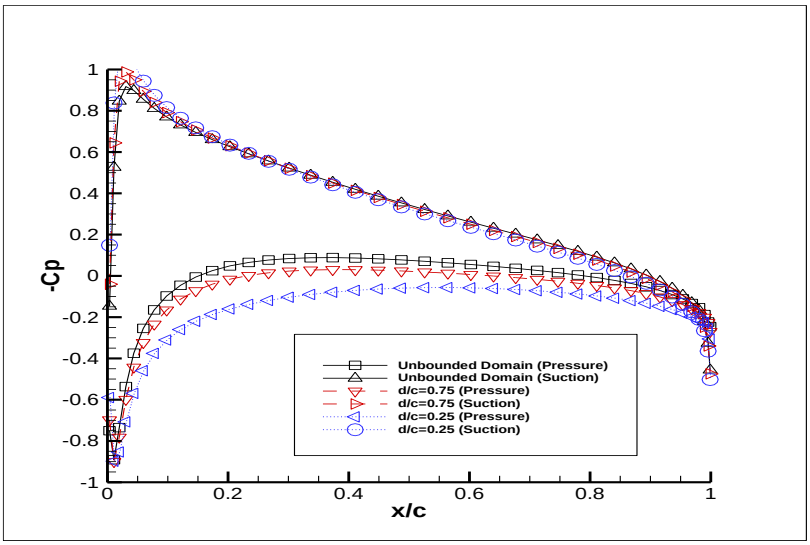

Fig. 5: Finite-depth effect on pressure distribution for mid-section of rectangular wing (AR=5).

Table 1. Geometrical details of tapered swept back wing.

2y/s	c/s	f_{max}/c	t_{max}/c
0.0 (Root section)	0.2000	0.0	0.1200
0.1	0.1867	0.0	0.1178
0.2	0.1733	0.0	0.1154
0.3	0.1600	0.0	0.1125
0.4	0.1467	0.0	0.1091
0.5	0.1333	0.0	0.1050
0.6	0.1200	0.0	0.1000
0.7	0.1067	0.0	0.0937
0.8	0.0933	0.0	0.0857
0.9	0.0800	0.0	0.0750
0.95	0.0733	0.0	0.0546
0.975	0.0700	0.0	0.0286
1.0 (Tip section)	0.0667	0.0	0.0000

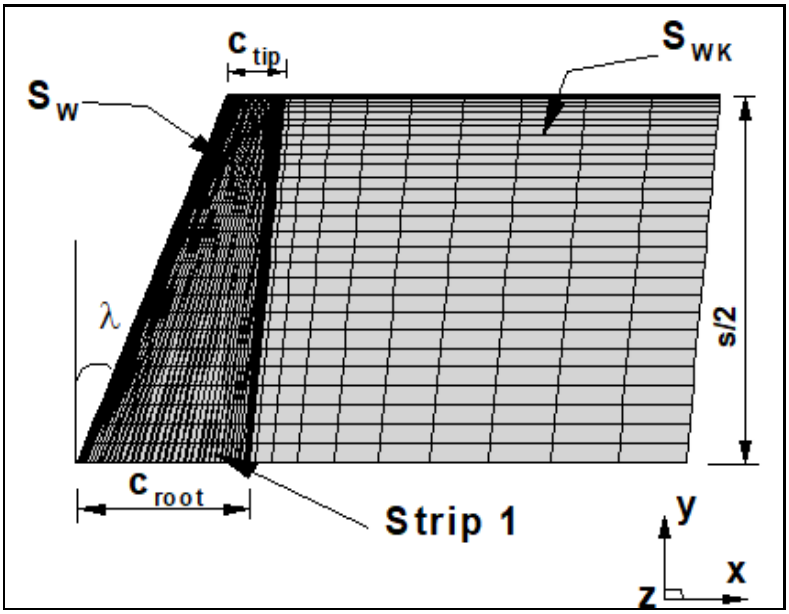

Fig. 6: Definitions of parameters and panels on tapered swept back wing and its wake, α=5º (Half of wing and its wake are shown due to symmetry).

In Fig. 7, the effects of finite depth on pressure distribution at root chord-based Froude number Fr_c=0.9 are shown for mid-section (Strip 1). The ratio of wing distance from free surface to root chord is (h/c_{root}=1.0). It is noted from this figure that smaller depth ratio of finite bottom (d/c_{root}=0.25) has a significant effect on the pressure distribution. In Table 2, the effects of finite-depth on lift and drag coefficients (induced drag + wave drag, including bottom effect for drag) are shown. It can be seen that the shallower finite-depth causes an increase in both lift and drag coefficients. This result is consistent with the pressure distribution shown in Fig. 7.

Table 2. Lift and drag coefficients at different finite-depth ratios.

d/c_{root}	C_L	C_D
100	0.2093	0.0047
0.75	0.2097	0.0046
0.25	0.5480	0.0091

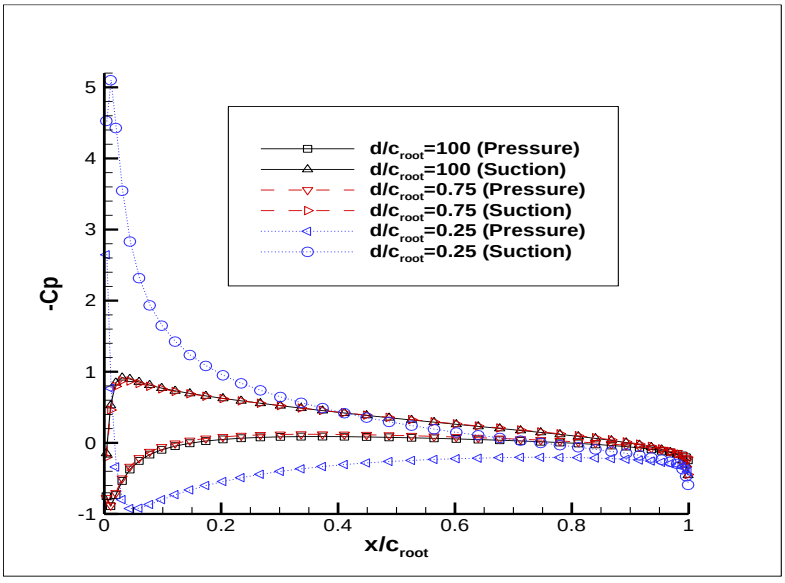

Fig. 7: Finite-depth effect on pressure distribution for Strip 1, h/c_{root}=1.0, Fr_c=0.9.

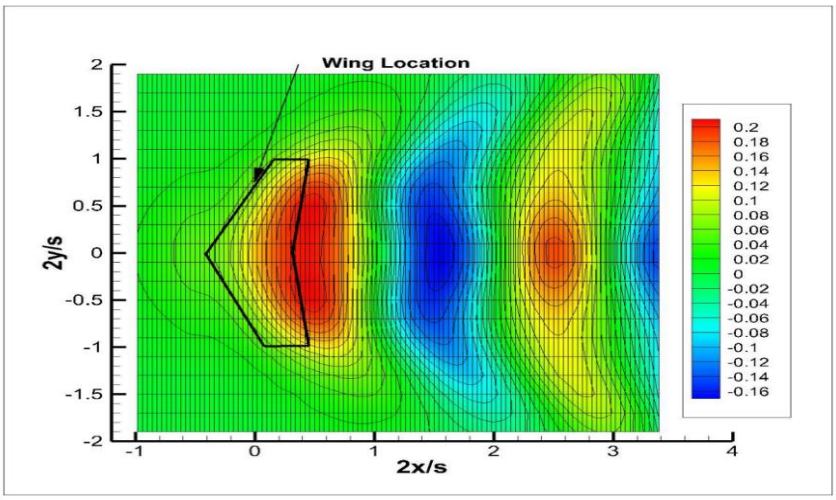

Fig. 8: 2-D wave contours on free surface, h/c_{root}=1.0, Fr_c=0.9.

The wave contours and free surface deformation for Fr_c=0.9 and h/c_{root}=1.0 are shown in Figs. 8 and 9, respectively. Notably, there is no finite-depth effect in this case. It is valued at noting that the presence of the Kelvin wave pattern observed in deep water. On the other hand, the wave contours are illustrated in Fig. 10, considering finite-depth effects, where the Kelvin wedge angle has now increased. In addition, both wave lengths and wave heights have also increased compared to those observed in the infinite depth case. This result correlates

with the increase loading on the wing surface, as demonstrated in Table 2 and Fig. 7. The dimensionless pressure distributions on the back side of wing in unbounded flow domain as well as with the effects of free surface and finite bottom, are shown in Figs 11 and 12, respectively. Similarly, the dimensionless pressure distributions on the face side of wing in unbounded flow domain and with the effects of free surface and finite bottom are illustrated in Figs 13 and 14, respectively. Notably, the differences are marginal for this particular case. Furthermore, the convergence history of the present IBEM is depicted for both pressure distributions on the mid-section and for lift and drag coefficients in Figs. 15 and 16, respectively. It is worth mentioning that the results presented in Figs 15 and 16 agree well with each other, and the converged solution is achieved by the second iteration step.

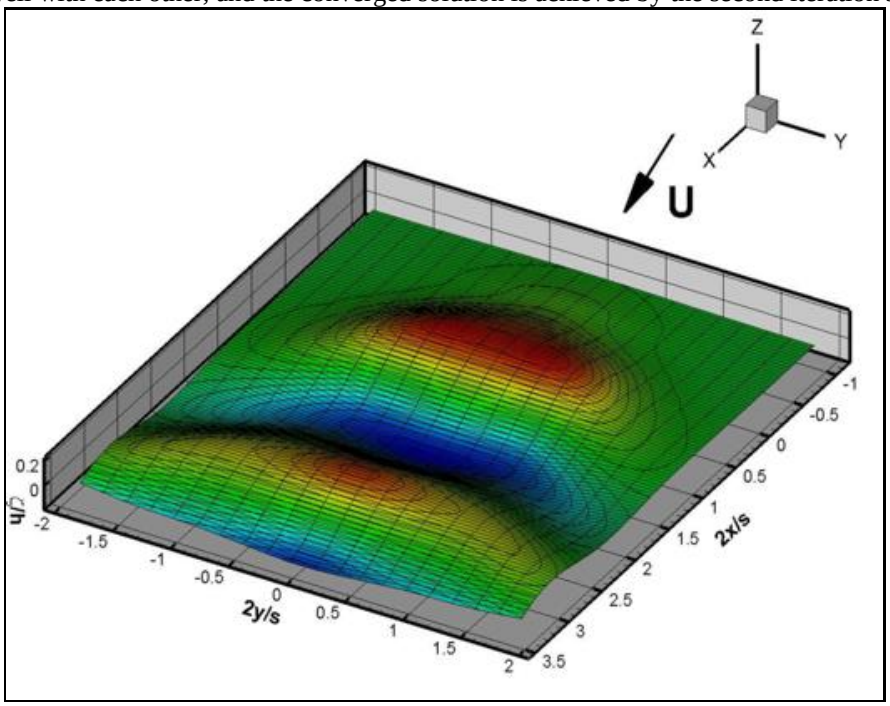

Fig. 9: 3-D wave deformation on free surface, h/c_{root}=1.0, Fr_c=0.9.

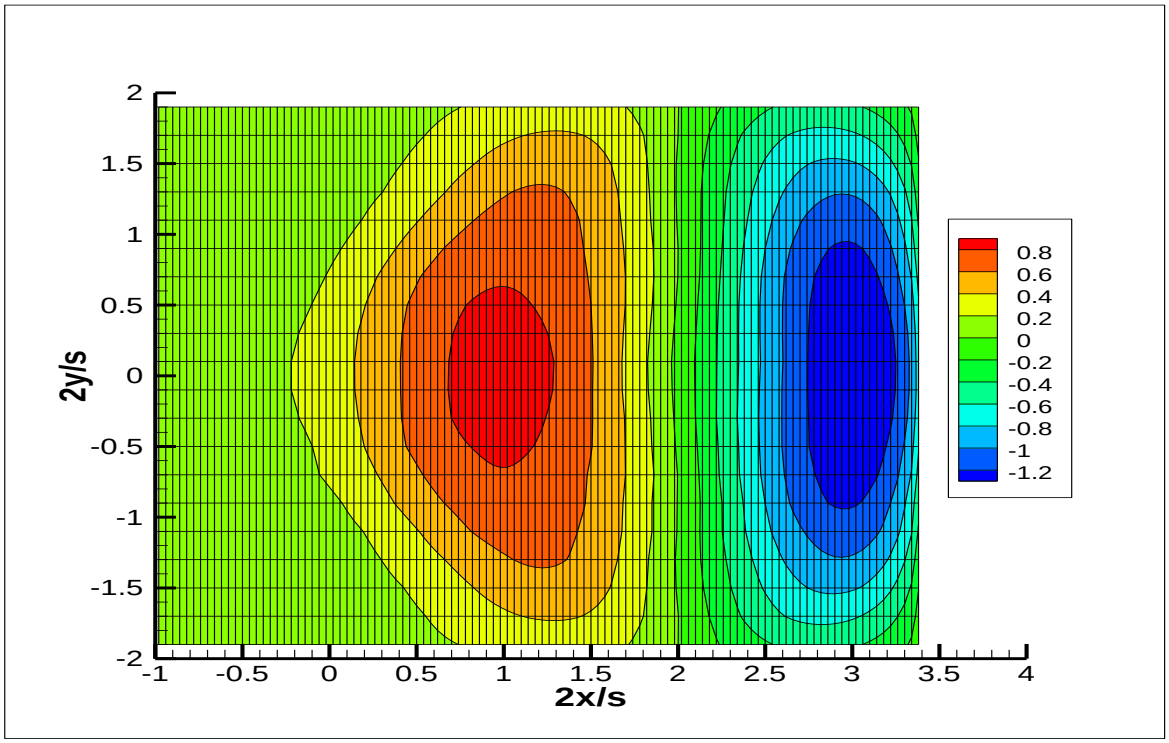

Fig. 10: Wave contours on free surface for h/c_{root}=1.0, Fr_c=0.9, d/c_{root}=0.25.

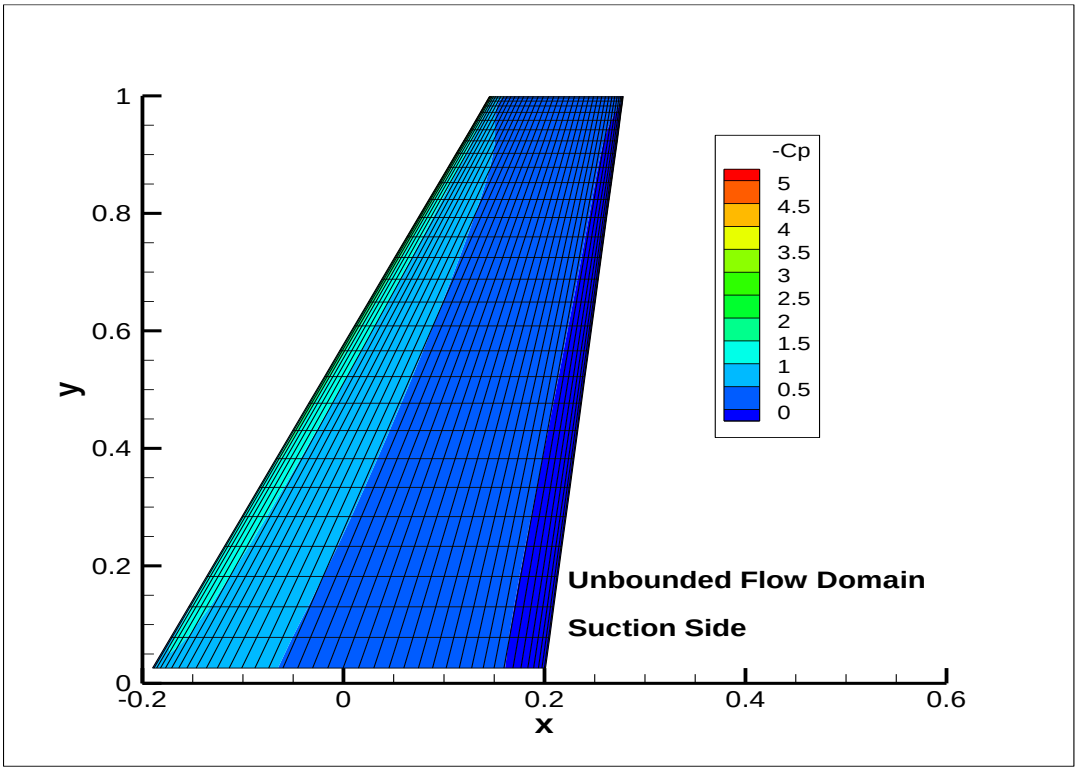

Fig. 11: Non-dimensional pressure distribution on suction side of wing in unbounded flow domain.

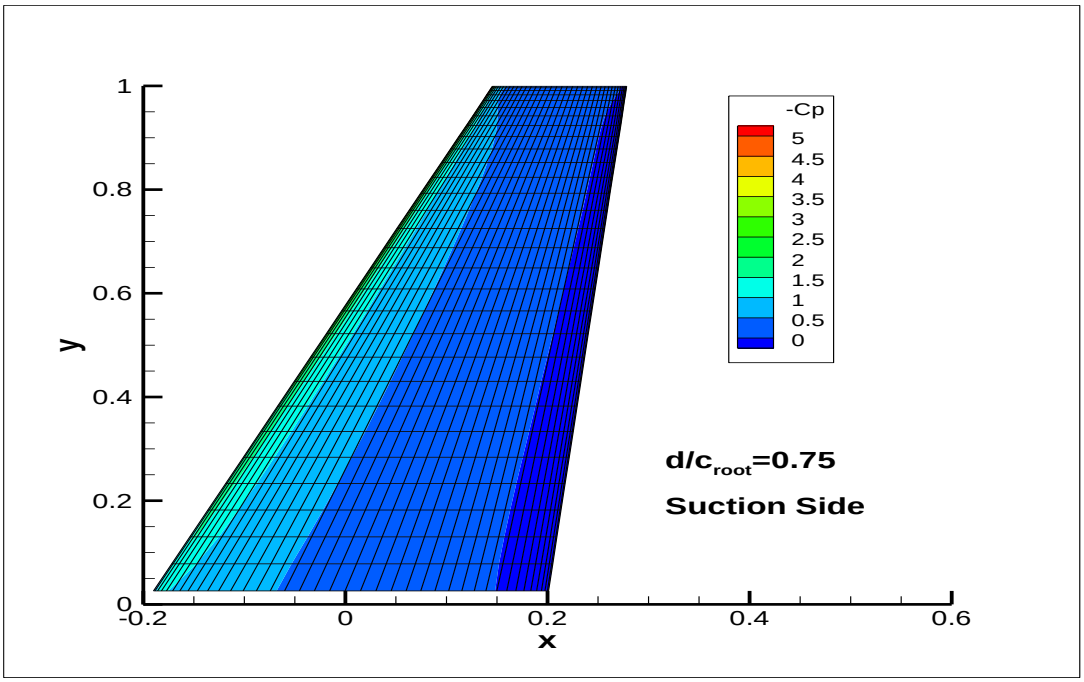

Fig. 12: Non-dimensional pressure distribution on suction side of wing with free surface and finite depth effects, $h/c_{root}=1.0$, $Fr_c=0.9$.

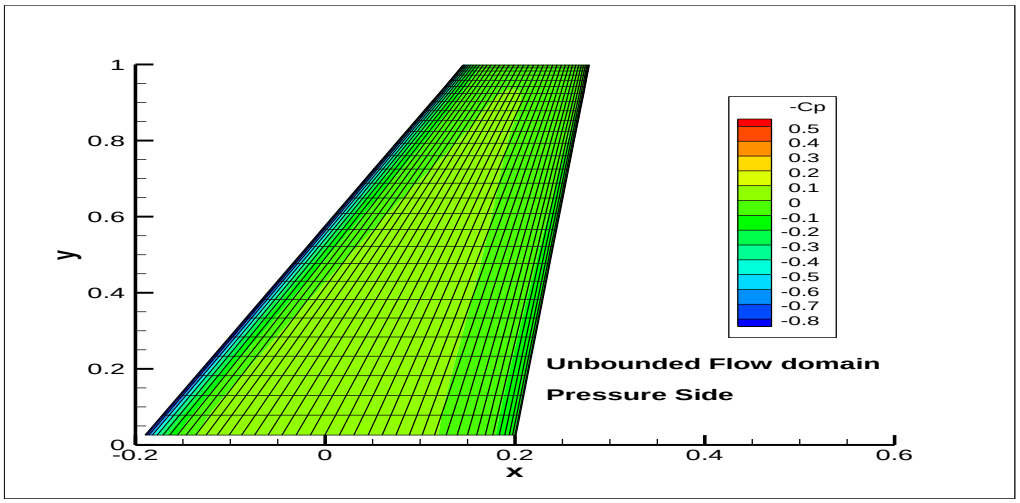

Fig. 13: Non-dimensional pressure distribution on pressure side of wing in unbounded flow domain.

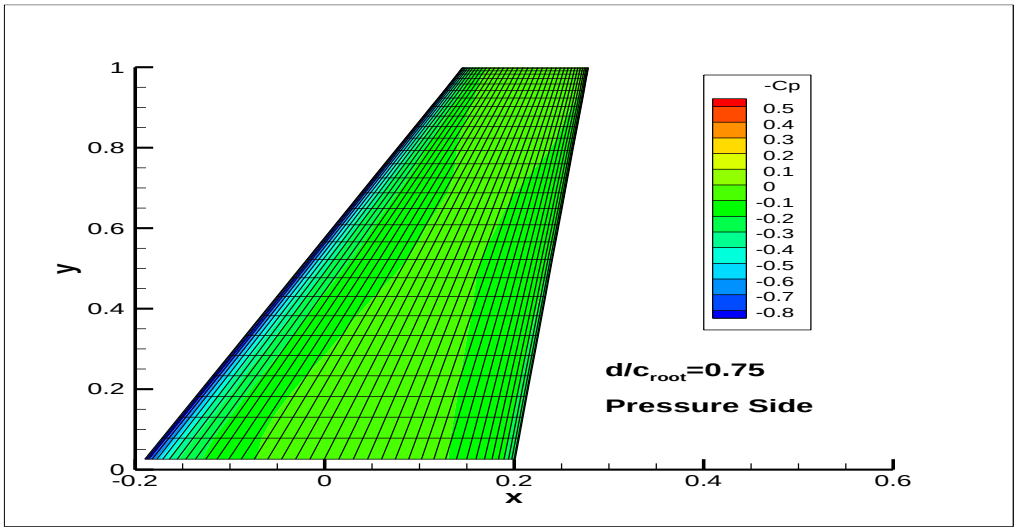

Fig. 14: Non-dimensional pressure distribution on pressure side of wing with free surface and finite depth effects, h/c_{root}=1.0, Fr_c=0.9.

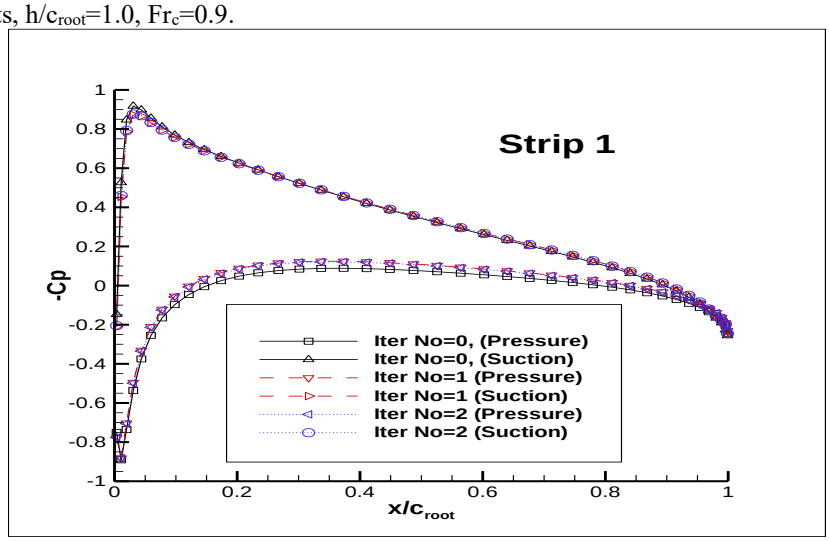

Fig. 15: Convergence history for pressure distribution, h/c_{root}=1.0, Fr_c=0.9, d/c_{root}=0.75.

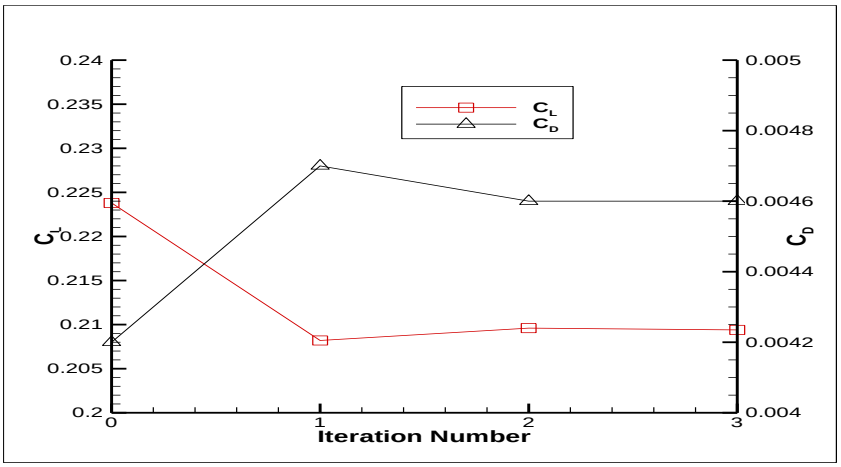

Fig. 16: Convergence of IBEM for lift and drag coefficients versus iteration number, h/c_{root}=1.0, Fr_c=0.9, d/c_{root}=0.75.

5. Conclusions

An iterative numerical method previously described has been adapted and extended to accommodate the movement of 3-D wings above a free water surface with finite depth. Some new numerical results have been presented. The procedure involved separate solutions for the wing, free surface, and bottom surface parts, with each problem iteratively influencing the others through their potential values. The method is based on the potential flow model, has no viscosity terms, and linearizes the free surface condition without accounting for wave breaking and spray effects in the calculations. The numerical method was first tested on a rectangular wing with a high aspect ratio, allowing for a comparison of pressure distribution on mid-section with that obtained from a 2-D panel method, serving as a validation test. NACA0012 sections were employed along the span-wise direction. A very good satisfactory agreement has been found between two results. The numerical method was then applied to a tapered swept back wing moving steadily over a free water surface with varying depths to assess its aero-hydrodynamic performance. The findings are follows:

1) The wing loading increases as the depth of bottom surface decreases.
2) In deep water, a Kelvin wave pattern emerges, with the Kelvin wedge angle increasing for shallower bottom surfaces, consistent with findings given in (Larsson and Raven, 2010).
3) Wave heights and lengths on the free surface also increase with shallower bottom depths, aligning with those of given in (Larsson and Raven, 2010).
4) The method demonstrates that very rapid convergence is obtained, say only a few iteration steps.

These results demonstrate the significant impact of finite bottom surfaces on the performance of 3-D wings, emphasizing the necessity of considering such effects during the early and final design phases of 3-D Wing-in-Ground effect vehicles.

References

Bal, S. (2007a): High-speed submerged and surface piercing cavitating hydrofoils, including tandem case, Ocean Engineering Vol. 34, pp. 1935-1946. http://dx.doi.org/10.1016/j.oceaneng. 2007.03.007.

Bal, S. (2007b): A numerical method for the prediction of wave pattern of surface piercing cavitating hydrofoils, Proceedings of the Institution of Mechanical Engineers, Part C, Journal of Mechanical Engineering Sciences, Vol. 221, No. 12, pp. 1623-1633. https://doi.org/10.1243/09544062JMES557.

Bal, S. (2011): The effect of finite depth on 2-D and 3-D cavitating hydrofoils, Journal of Marine Science and Technology, Vol. 6, No. 2, pp. 129-142. https://doi.org/ 10.1007/s00773-011-0117-2.

Bal, S. (2016): Free surface effects on 2-D airfoils and 3-D wings moving over water, Ocean Systems Engineering, An International Journal, Vol. 6, No. 3, pp. 245-264. https://doi.org/10.12989/ose.2016.6.3.245.

Bal, S. (2018): Prediction of hydrodynamic performance of 3-D WIG by IBEM, International Journal of Maritime Engineering, (RINA Transactions Part A), Vol. 160, pp. 249-256.

https://doi.org/10.5750/ijme.v160iA3.1062.

Bal, S. (2023): Numerical investigation of curved tip effect on the performance of 3-D cavitating hydrofoils moving under free surface, Journal of Sailing Technology, SNAME, Vol. 8, No. 1, pp. 39-64. https://doi.org/10.5957/jst/2023.8.3.39.

Bal, S., Kinnas, S.A. and Lee, H. (2001): Numerical analysis of 2-D and 3-D cavitating hydrofoils under a free surface, Journal of Ship Research, Vol. 45, No. 1, pp. 34-49. https://doi.org/10.5957/jsr.2001.45.1.34.

Bal, S. and Kinnas, S.A. (2002): A BEM for the prediction of free surface effect on cavitating hydrofoils, Computational Mechanics, Vol. 28, pp. 260-274. https://doi.org/10.1007/s00466-001-0286-7.

Barber, J.T. (2007): A study of water surface deformation due to tip vortices of a wing-in-ground effect, Journal of Ship Research, Vol. 51, No. 2, pp. 182-186. https://doi.org/10.5957/jsr.2007.51.2.182.

Carabineanu, A. (2014): The study of the potential flow past a submerged hydrofoil by the complex boundary element method, Engineering Analysis with Boundary Elements, Vol. 39, pp. 23-35. https://doi.org/10.1016/j.enganabound.2013.10.017.

Chen, Z.M. (2012): A vortex-based panel method for potential flow simulation around a hydrofoil, Journal of Fluids and Structures, Vol. 28, pp. 378-391. https://doi.org/10.1016/j.jfluidstructs.2011.10.003.

Grundy, I. (1986): Airfoils moving in air close to a dynamic water surface, Journal of the Australian Mathematical Society Series B, Vol. 27, No. 3, pp. 327-345. https://doi.org/10.1017/S0334270000004963.

Jung, J.H., Kim, M.J., Yoon, H.S., Hung, P.A., Chun, H.H. and Park, D.W. (2012): Endplate effect on aerodynamic characteristics of three-dimensional wings in close free surface proximity, International Journal of Naval Architecture and Ocean Engineering, Vol. 4, pp. 477-487.

https://doi.org/10.2478/IJNAOE-2013-0112.

Katz, J. and Plotkin, A. (2001): Low Speed Aerodynamics, 2nd Edition, Cambridge University Press, NY, USA.

Kinnas, S.A. and Hsin, C.Y. (1992): A boundary element method for the analysis of the unsteady flow around extreme propeller geometries, AIAA Journal, Vol. 30, pp. 688-696. https://doi.org/10.2514/3.10973.

Larsson, L. and Raven, H.C. (2010): Ship Resistance and Flow (Editor: Paulling, J.R.), SNAME, NJ, USA.

Liang, H. and Zong, Z. (2011): A subsonic lifting surface theory for wing-in-ground effect, Acta Mechanica, Vol. 219, pp. 203-217. https://doi.org/10.1007/s00707-011-0444-8.

Matveev, K.I. (2013): Modeling of finite-span ram wings moving above water of finite Froude numbers, Journal of Ship Research, Vol. 58, no. 3, pp. 146–156.http://dx.doi.org/10.5957/JOSR.58.3.130046.

Rozhdestvensky, K.V. (2006): Wing-in-ground effect vehicles, Progress in Aerospace Sciences, Vol. 42, pp. 211–283. https://doi.org/10.1016/j.paerosci.2006.10.001.

Rozhdestvensky, K.V. (2010): Aerodynamics of a Lifting System in Extreme Ground Effect, Springer-Verlag Berlin and Heidelberg GmbH & Co. K, Germany. https://doi.org/10.1007/978-3-662-04240-3.

Sun, S.Y. and Wu, G.X. (2022): Inviscid flow passing a lifting body with a higher order boundary element method, Engineering Analysis with Boundary Elements, Vol. 136, pp. 144-157.

https://doi.org/10.1016/j.enganabound.2021.12.012.

Zong, Z., Liang, H. and Zhou, L. (2012): Lifting line theory for wing-in ground effect in proximity to a free surface, Journal of Engineering Mathematics, Vol. 74, pp. 143-158.

https://doi.org/10.1007/s10665-011-9497-x.